



# BASS. XLII. The Relation between the Covering Factor of Dusty Gas and the Eddington Ratio in Nearby Active Galactic Nuclei

C. Ricci<sup>1,2</sup>, K. Ichikawa<sup>3</sup>, M. Stalevski<sup>4,5</sup>, T. Kawamuro<sup>6</sup>, S. Yamada<sup>6</sup>, Y. Ueda<sup>7</sup>, R. Mushotzky<sup>8,9</sup>, G. C. Privon<sup>10,11</sup>, M. J. Koss<sup>12,13</sup>, B. Trakhtenbrot<sup>14</sup>, A. C. Fabian<sup>15</sup>, L. C. Ho<sup>2,16</sup>, D. Asmus<sup>17,18</sup>, F. E. Bauer<sup>19,20,21</sup>, C. S. Chang<sup>22</sup>, K. K. Gupta<sup>23</sup>, K. Oh<sup>24</sup>, M. Powell<sup>25,26</sup>, R. W. Pfeifle<sup>27,28</sup>, A. Rojas<sup>1,29</sup>, F. Ricci<sup>30</sup>, M. J. Temple<sup>1</sup>, Y. Toba<sup>31,32,33</sup>, A. Tortosa<sup>34</sup>, E. Treister<sup>19</sup>, F. Harrison<sup>35</sup>, D. Stern<sup>36</sup>, and C. M. Urry<sup>37</sup>

<sup>1</sup> Instituto de Estudios Astrofísicos, Facultad de Ingeniería y Ciencias, Universidad Diego Portales, Avenida Ejército Libertador 441, Santiago, Chile  
[claudio.ricci@mail.udp.cl](mailto:claudio.ricci@mail.udp.cl)

<sup>2</sup> Kavli Institute for Astronomy and Astrophysics, Peking University, Beijing 100871, People's Republic of China

<sup>3</sup> Frontier Research Institute for Interdisciplinary Sciences, Tohoku University, Sendai, 980-8578, Japan

<sup>4</sup> Astronomical Observatory, Volgina 7, 11060 Belgrade, Serbia

<sup>5</sup> Sterrenkundig Observatorium, Universiteit Ghent, Krijgslaan 281 S9, B-9000 Ghent, Belgium

<sup>6</sup> RIKEN Cluster for Pioneering Research, 2-1 Hirosawa, Wako, Saitama 351-0198, Japan

<sup>7</sup> Department of Astronomy, Kyoto University, Kitashirakawa -Oiwake-cho, Sakyo-ku, Kyoto 606-8502, Japan

<sup>8</sup> Department of Astronomy, University of Maryland, College Park, MD 20742, USA

<sup>9</sup> Joint Space-Science Institute, University of Maryland, College Park, MD 20742, USA

<sup>10</sup> National Radio Astronomy Observatory, 520 Edgemont Road, Charlottesville, VA 22903, USA

<sup>11</sup> Department of Astronomy, University of Florida, PO Box 112055, Gainesville, FL 32611, USA

<sup>12</sup> Eureka Scientific, 2452 Delmer Street, Suite 100, Oakland, CA 94602-3017, USA

<sup>13</sup> Space Science Institute, 4750 Walnut Street, Suite 205, Boulder, CO 80301, USA

<sup>14</sup> School of Physics and Astronomy, Tel Aviv University, Tel Aviv 69978, Israel

<sup>15</sup> Institute of Astronomy, Madingley Road, Cambridge CB3 0HA, UK

<sup>16</sup> Department of Astronomy, School of Physics, Peking University, Beijing 100871, People's Republic of China

<sup>17</sup> Department of Physics & Astronomy, University of Southampton, Southampton, SO17 1BJ, UK

<sup>18</sup> Gymnasium Schwarzenbek, D-21493 Schwarzenbek, Germany

<sup>19</sup> Instituto de Astrofísica, Facultad de Física, Pontificia Universidad Católica de Chile, Campus San Joaquín, Av. Vicuña Mackenna 4860, Macul Santiago, 7820436, Chile

<sup>20</sup> Centro de Astroingeniería, Facultad de Física, Pontificia Universidad Católica de Chile, Campus San Joaquín, Av. Vicuña Mackenna 4860, Macul Santiago, 7820436, Chile

<sup>21</sup> Millennium Institute of Astrophysics, Nuncio Monseñor Sótero Sanz 100, Of 104, Providencia, Santiago, Chile

<sup>22</sup> Joint ALMA Observatory, Avenida Alonso de Cordova 3107, Vitacura 7630355, Santiago, Chile

<sup>23</sup> STAR Institute, Quartier Agora—Allée du six Août, 19c B-4000 Liège, Belgium

<sup>24</sup> Korea Astronomy & Space Science Institute, 776, Daedeokdae-ro, Yuseong-gu, Daejeon 34055, Republic of Korea

<sup>25</sup> Kavli Institute for Particle Astrophysics and Cosmology, Stanford University, 452 Lomita Mall, Stanford, CA 94305, USA

<sup>26</sup> Department of Physics, Stanford University, 382 Via Pueblo Mall, Stanford, CA 94305, USA

<sup>27</sup> X-Ray Astrophysics Laboratory, NASA Goddard Space Flight Center, Code 662, Greenbelt, MD 20771, USA

<sup>28</sup> Oak Ridge Associated Universities, NASA NPP Program, Oak Ridge, TN 37831, USA

<sup>29</sup> Centro de Astronomía (CITEVA), Universidad de Antofagasta, Avenida Angamos 601, Antofagasta, Chile

<sup>30</sup> Dipartimento di Matematica e Fisica, Università Roma Tre, via della Vasca Navale 84, I-00146, Roma, Italy

<sup>31</sup> National Astronomical Observatory of Japan, 2-21-1 Osawa, Mitaka, Tokyo 181-8588, Japan

<sup>32</sup> Academia Sinica Institute of Astronomy and Astrophysics, 11F Astronomy-Mathematics Building, AS/NTU, No.1, Section 4, Roosevelt Road, Taipei 10617, Taiwan

<sup>33</sup> Research Center for Space and Cosmic Evolution, Ehime University, 2-5 Bunkyo-cho, Matsuyama, Ehime 790-8577, Japan

<sup>34</sup> INAF—Osservatorio Astronomico di Roma, via di Frascati 33, I-00078 Monte Porzio Catone, Italy

<sup>35</sup> Cahill Center for Astronomy and Astrophysics, California Institute of Technology, Pasadena, CA 91125, USA

<sup>36</sup> Jet Propulsion Laboratory, California Institute of Technology, 4800 Oak Grove Drive, MS 169-224, Pasadena, CA 91109, USA

<sup>37</sup> Yale Center for Astronomy & Astrophysics, Physics Department, PO Box 208120, New Haven, CT 06520-8120, USA

Received 2023 August 27; revised 2023 October 19; accepted 2023 October 23; published 2023 December 1

## Abstract

Accreting supermassive black holes (SMBHs) located at the centers of galaxies are typically surrounded by large quantities of gas and dust. The structure and evolution of this circumnuclear material can be studied at different wavelengths, from the submillimeter to the X-ray. Recent X-ray studies have shown that the covering factor of the obscuring material tends to decrease with increasing Eddington ratio, likely due to radiative feedback on dusty gas. Here we study a sample of 549 nearby ( $z \lesssim 0.1$ ) hard X-ray (14–195 keV) selected nonblazar active galactic nuclei (AGN) and use the ratio between the AGN infrared and bolometric luminosity as a proxy of the covering factor. We find that, in agreement with what has been found by X-ray studies of the same sample, the covering factor decreases with increasing Eddington ratio. We also confirm previous findings that showed that obscured AGN typically have larger covering factors than unobscured sources. Finally, we find that the median covering factors of AGN located in different regions of the column density–Eddington ratio diagram are in good agreement with what would be expected from a radiation-regulated growth of SMBHs.



Original content from this work may be used under the terms of the [Creative Commons Attribution 4.0 licence](https://creativecommons.org/licenses/by/4.0/). Any further distribution of this work must maintain attribution to the author(s) and the title of the work, journal citation and DOI.

*Unified Astronomy Thesaurus concepts:* Active galaxies (17); Seyfert galaxies (1447); Infrared photometry (792); X-ray astronomy (1810); Quasars (1319)

## 1. Introduction

Supermassive black holes (SMBHs) that accrete copious amounts of gas and dust from their surroundings can emit throughout the whole electromagnetic spectrum and are observed as active galactic nuclei (AGN). The material responsible for most of the AGN obscuration is widely believed to be anisotropically distributed, possibly in the form of a torus, as predicted by the classical AGN unification model (Antonucci 1993; Urry & Padovani 1995; Netzer 2015; Ramos Almeida & Ricci 2017; Hickox & Alexander 2018). This obscuring material can be studied in the X-ray band in absorption (e.g., Awaki et al. 1991; Ueda et al. 2003; Merloni et al. 2014; Ricci et al. 2015) and/or through spectral features (e.g., Lightman & White 1988; Pounds et al. 1990; Matt et al. 1991), in the infrared (IR) from the radiation produced by reprocessing of the UV/optical and X-ray radiation in circumnuclear dust (e.g., Krolik & Begelman 1988; Granato & Danese 1994; Jaffe et al. 2004; Elitzur 2008; Gandhi et al. 2009; Alonso-Herrero et al. 2011; Ramos Almeida et al. 2011; Lanz et al. 2019; Gámez Rosas et al. 2022), or at millimeter wavelengths from dust continuum and molecular line emission (e.g., García-Burillo et al. 2019; Impellizzeri et al. 2019; Imanishi et al. 2020; García-Burillo et al. 2021; Tristram et al. 2022). Understanding the structure and evolution of the gas and dust surrounding these accreting SMBHs is extremely important, because this is likely to be the reservoir of material that eventually accretes onto SMBHs. Moreover, being located in the inner regions of the accreting system, this material could carry imprinted signatures of AGN feedback (e.g., Fabian et al. 2006; Ricci et al. 2017a), which is thought to play an important role in the evolution of galaxies (e.g., Kormendy & Ho 2013; Harrison 2017 and references therein).

One of the main parameters of the obscuring material surrounding the SMBH is its covering factor (e.g., Lawrence & Elvis 2010), i.e., the fraction of the SMBH sky that is obscured, which can be inferred using the following techniques in the X-ray, optical, and IR.

- (i) In X-ray surveys using the fraction of obscured sources ( $f_{\text{obs}}$ ; e.g., Ueda et al. 2003, 2014; La Franca et al. 2005; Hasinger 2008; Merloni et al. 2014), i.e., the fraction of AGN with column densities  $\log(N_{\text{H}}/\text{cm}^{-2}) \geq 22$ . According to the unification model, different objects would probe different inclination angles with respect to the torus. Therefore, if the sample has a high completeness level, the fraction of sources within a certain range of column densities is a proxy of the mean covering factor of the obscuring material with that column density. Alternatively, the fraction of AGN optically classified as type 1 (i.e., showing both broad permitted and narrow forbidden optical lines) and type 2 (displaying only narrow lines) can also be used to infer the covering factor of the obscuring material (e.g., Lawrence & Elvis 1982; Simpson 2005; Toba et al. 2013; Oh et al. 2015). However, a possible source of uncertainty related to this approach is the existence of a fraction of AGN that are optically dull (e.g., Georgantopoulos & Georgakakis 2005; Smith et al. 2014; Koss et al. 2017) and of unobscured sources in which the

optical broad lines are too faint or broad to be detected (e.g., Bianchi et al. 2017).

- (ii) From the ratio between the IR and the bolometric AGN luminosity. Considering that a significant fraction of the IR emission in AGN is produced by dust reprocessing, it has been argued that the fraction of bolometric luminosity ( $L_{\text{Bol}}$ ) reemitted in the IR is directly proportional to the covering factor of the obscuring material (e.g., Maiolino et al. 2007; Treister et al. 2008; Gandhi et al. 2009; Assef et al. 2013; Netzer et al. 2016; Toba et al. 2021). However, a detailed study carried out using radiative transfer simulations of dusty tori (Stalevski et al. 2016) has shown that the relation between the covering factor and the ratio between the IR and bolometric AGN luminosity is significantly more complex than previously believed (see Section 3).
- (iii) From torus models applied to the mid-IR spectral energy distribution (SED) of individual AGN. Several IR torus models have been developed in the past decade (Hönig et al. 2006, 2010; Schartmann et al. 2008; Hönig & Kishimoto 2010; Stalevski et al. 2012, 2016; Siebenmorgen et al. 2015; Hönig & Kishimoto 2017) and can be used to recover some of the properties of the dust surrounding SMBHs, including its covering factor. Works carried out using torus models such as CLUMPY (Nenkova & Sirocky 2008a; Nenkova et al. 2008b; Nikutta et al. 2009), CAT3D (Hönig & Kishimoto 2010), and CAT3D-WIND (Hönig & Kishimoto 2017) have been applied to a significant number of AGN (e.g., Mor et al. 2009; Alonso-Herrero et al. 2011, 2021; Ramos Almeida et al. 2011; Ichikawa et al. 2015; Zhuang et al. 2018; García-Bernete et al. 2019; González-Martín et al. 2019; García-Bernete et al. 2022). For one of the closest AGN, the Circinus galaxy, it has been possible to infer the covering factor by modeling both spectroscopic and high-resolution morphological data (Stalevski et al. 2017, 2019).
- (iv) Applying torus models to the broadband X-ray spectra of AGN. X-ray torus models (e.g., Murphy & Yaqoob 2009; Brightman & Nandra 2011; Liu & Li 2014; Paltani & Ricci 2017; Baloković et al. 2018; Tanimoto et al. 2019; Buchner et al. 2021; Ricci & Paltani 2023), some of which now include the effect of dusty gas in the X-ray (Ricci & Paltani 2023; Vander Meulen et al. 2023), allow us to infer the covering factor of the gas and dust surrounding the SMBH. This has been particularly effective in recent years using NuSTAR observations (e.g., Brightman et al. 2015; Ogawa et al. 2019; Tanimoto et al. 2020; Zhao et al. 2020; Ogawa et al. 2021; Uematsu et al. 2021; Yamada et al. 2021; Andonie et al. 2022; Inaba et al. 2022), since its large energy coverage (3–79 keV) allows for the detection of both main features produced by reprocessed X-ray radiation: the Fe  $K\alpha$  line (6.4 keV) and the Compton hump ( $\sim 30$  keV).

A relation between the torus covering factor and the AGN luminosity was originally found by the decrease in the fraction of type 2 AGN with the luminosity (Lawrence & Elvis 1982; Lawrence 1991). Studies of X-ray (e.g., Ueda et al. 2003;

Treister & Urry 2005, 2006; Sazonov et al. 2007; Della Ceca et al. 2008; Hasinger 2008; Beckmann et al. 2009; Ueda et al. 2011; Merloni et al. 2014; Ueda et al. 2014; Buchner et al. 2015) and IR (e.g., Maiolino et al. 2007; Treister et al. 2008; Gandhi et al. 2009; Assef et al. 2013; Lusso et al. 2013; Toba et al. 2014; Lacy et al. 2015; Mateos et al. 2016; Stalevski et al. 2016; Ichikawa et al. 2017) surveys, as well as IR studies carried out by applying torus models (e.g., Mor et al. 2009; Alonso-Herrero et al. 2011), have confirmed this trend. The relationship between the covering factor of the obscuring material and the luminosity has been shown to be related to the intrinsically different luminosity functions of obscured and unobscured AGN (e.g., Della Ceca et al. 2008; Tueller et al. 2008; Burlon et al. 2011), and it can reproduce the decrease of the Fe K $\alpha$  intensity with luminosity (Ricci et al. 2013, see also Iwasawa & Taniguchi 1993; Bianchi et al. 2007; Ricci et al. 2014; Boorman et al. 2018; Matt & Iwasawa 2019). Recently, it has been shown that the main driver of this correlation could be the Eddington ratio (Ricci et al. 2017a, 2022a; see also Buchner & Bauer 2017; Ezhikode et al. 2017; Ananna et al. 2022a), with radiation pressure on dusty gas (e.g., Fabian et al. 2006; Venanzi et al. 2020) likely responsible for the decrease of the covering factor with increasing mass-normalized accretion rates. Here we complement our previous X-ray studies (Ricci et al. 2017a, 2022a) by analyzing the relation between the dust covering factor, obtained by comparing IR to bolometric luminosities, and the Eddington ratio for sources from the BAT AGN Spectroscopic Survey (BASS<sup>38</sup>; Ricci et al. 2017b; Koss et al. 2017, 2022a). Throughout the paper, we adopt standard cosmological parameters ( $H_0 = 70 \text{ km s}^{-1} \text{ Mpc}^{-1}$ ,  $\Omega_m = 0.3$ ,  $\Omega_\Lambda = 0.7$ ).

## 2. Sample and Data

Our sample is composed of objects from BASS. BASS is studying in detail the multiwavelength properties of AGN detected by the Burst Alert Telescope (BAT; Barthelmy et al. 2005) on board the Neil Gehrels Swift Observatory (Gehrels et al. 2004) with the goal of improving our understanding of the properties of accreting SMBHs in the local Universe ( $z \lesssim 0.1$ ). Swift/BAT operates in a band (14–195 keV) that is not significantly affected by obscuration up to column densities  $\log(N_{\text{H}}/\text{cm}^{-2}) \simeq 24$  (e.g., Figure 1 in Ricci et al. 2015; see also Koss et al. 2016), thus providing an almost unbiased view of local AGN. Swift/BAT has detected 733 nonblazar AGN in the first 70 months of operations (Baumgartner et al. 2013; Ricci et al. 2017b), and our initial sample consists of the 731 sources for which X-ray spectroscopy was available. The intrinsic 14–150 keV AGN luminosities ( $L_{14-150}$ ) and their column densities are taken from Ricci et al. (2017b), who reported the broadband (0.3–150 keV) X-ray spectral properties of the AGN from the Swift/BAT 70 month catalog. The 1–1000  $\mu\text{m}$  luminosity of the torus ( $L_{\text{Tor}}$ ), necessary to estimate its covering factor (Section 3), was calculated from the 12  $\mu\text{m}$  AGN luminosity ( $L_{12\mu\text{m}}$ ) reported in Ichikawa et al. (2019) using a correction factor of  $\kappa_{\text{IR}} = 2.92$  (i.e.,  $L_{\text{Tor}} = \kappa_{\text{IR}} \times L_{12\mu\text{m}}$ ), based on the model of Stalevski et al. (2016). The AGN IR luminosities of Ichikawa et al. (2019) were obtained by the spectral decomposition of the IR SED, considering both AGN and host galaxy emission using DECOMPIR (Mullaney et al. 2011), and are shown to be in good agreement with the

luminosities obtained by high spatial resolution IR studies (e.g., Asmus et al. 2014; see Figure 11 of Ichikawa et al. 2019). Ichikawa et al. (2019) report IR luminosities for 587 nonblazar AGN, of which 21 only have upper limits, since their IR SED is dominated by other physical processes, such as star formation.

The black hole masses ( $M_{\text{BH}}$ ) for the sources of the BASS sample are listed in Koss et al. (2017, 2022b), who reported black hole masses for 790 AGN from the Swift/BAT 70 month catalog (Baumgartner et al. 2013). For unobscured AGN, black hole masses were mostly estimated using broad H $\alpha$  and H $\beta$  lines, while for obscured objects, we used black hole masses mostly estimated with velocity dispersion (see Koss et al. 2022b, 2022c for details). Similarly to what was done in Ricci et al. (2017a), we excluded the objects with  $N_{\text{H}} \geq 10^{22} \text{ cm}^{-2}$  for which  $M_{\text{BH}}$  was obtained using broad H $\alpha$  and H $\beta$ , since the black hole masses are likely underestimated because of the extinction of the optical emission (e.g., Ricci et al. 2022b; Mejía-Restrepo et al. 2022). Cross-matching the 587 AGN with available  $L_{\text{Tor}}$  with those for which we have  $M_{\text{BH}}$ , we obtain a final sample of 549 objects, of which 289 are unobscured [ $\log(N_{\text{H}}/\text{cm}^{-2}) < 22$ ] and 260 are obscured [ $\log(N_{\text{H}}/\text{cm}^{-2}) \geq 22$ ] AGN. For 19 of these objects, only an upper limit on  $L_{\text{Tor}}$  is available.

For all objects in our final sample, the intrinsic 14–150 keV and 12  $\mu\text{m}$  luminosities were calculated using the redshifts and redshift-independent distances reported in Koss et al. (2022b). We calculated the Eddington ratio  $\lambda_{\text{Edd}}$  from the Eddington luminosity,  $L_{\text{Edd}} = \frac{4\pi GM_{\text{BH}}m_{\text{p}}c}{\sigma_{\text{T}}}$ , where  $G$  is the gravitational constant,  $m_{\text{p}}$  is the mass of the proton,  $c$  is the speed of light, and  $\sigma_{\text{T}}$  is the Thomson cross section. The bolometric luminosity was calculated by either adopting the  $\lambda_{\text{Edd}}$ -dependent 2–10 keV bolometric corrections of Vasudevan & Fabian (2017;  $\kappa_{2-10} = \kappa(\lambda_{\text{Edd}})$ ) or considering a 14–150 keV bolometric correction of  $\kappa_{14-150} = 8.48$  ( $L_{\text{Bol}} = \kappa_{14-150} \times L_{14-150}$ ). The latter is equivalent to a 2–10 keV bolometric correction of  $\kappa_{2-10} = 20$  (Vasudevan & Fabian 2007) for an X-ray photon index of  $\Gamma = 1.8$ , consistent with the typical value of Swift/BAT AGN (Ricci et al. 2017b). The  $\lambda_{\text{Edd}}$ -dependent 2–10 keV bolometric corrections of Vasudevan & Fabian were implemented as in Ricci et al. (2017a), considering  $\kappa_{2-10} = 20$  for  $\lambda_{\text{Edd}} \leq 0.04$  and  $\kappa_{2-10} = 70$  for  $\lambda_{\text{Edd}} \geq 0.4$  and following  $\kappa_{2-10} \propto \lambda_{\text{Edd}}^{0.54}$  over the range  $0.04 < \lambda_{\text{Edd}} < 0.4$ . To also consider objects for which only an upper limit in  $L_{\text{Tor}}$  is available, all medians were calculated with the Kaplan–Meier estimator within the ASURV package (Feigelson & Nelson 1985; Isobe et al. 1986) using a PYTHON implementation (see Section 5 in Shimizu et al. 2016 for details). We also verified our results using other PYTHON implementation of the survival analysis approach, such as SCIKIT-SURVIVAL (Pölsterl 2020).

## 3. The Covering Factor of Dust

While most studies carried out in the past decade have used

$$R \equiv L_{\text{Tor}}/L_{\text{Bol}} \quad (1)$$

as a direct proxy of the covering factor of the circumnuclear dust (CF), Stalevski et al. (2016) have shown that the covering factor of the torus is not directly proportional to  $R$ ; instead, it is related by a more complex function due to the radiative transfer effects. In particular, Stalevski et al. (2016) illustrated how the anisotropic emission of both the accretion disk and the dusty

<sup>38</sup> [www.bass-survey.com](http://www.bass-survey.com)

torus plays a strong role in the relation between  $R$  and CF. The authors showed that  $R$  overestimates high covering factors and underestimates low covering factors for unobscured AGN while always underestimating the covering factors for obscured sources. Stalevski et al. (2016) provide corrections to take all of these effects into account (see Table 1 of their paper). These corrections do not yet take into account the effect of the SMBH spin, which could also change the radiation pattern of the accretion flow (e.g., Campitiello et al. 2018; Ishibashi et al. 2019). Here we will focus on the dust covering factors obtained by applying the corrections suggested by Stalevski et al. (2016). These corrections are given in the form of polynomials of  $R$  and depend on the optical depth of the silicate feature ( $\tau_{9.7}$ ) and whether the disk and the torus are misaligned. For pole-on (i.e., unobscured) objects, the covering factor of the dust is given by

$$CF^{\text{unobs}} = a_4 R^4 + a_3 R^3 + a_2 R^2 + a_1 R + a_0, \quad (2)$$

while for edge-on (i.e., obscured) AGN,

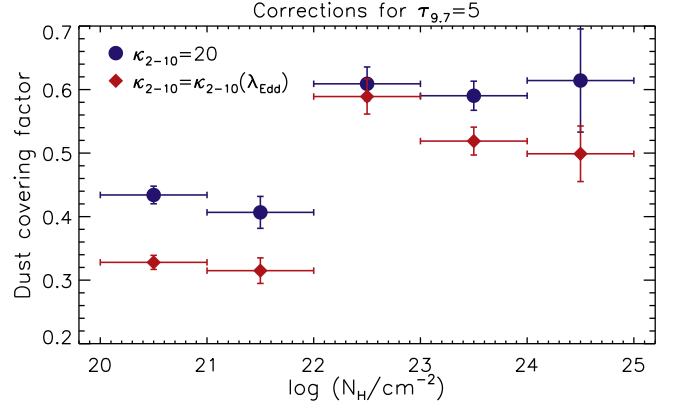
$$CF^{\text{obs}} = b_3 R^3 + b_2 R^2 + b_1 R + b_0. \quad (3)$$

We considered here  $\tau_{9.7} = 5$ , and, following the prescriptions of Stalevski et al. (2016), we set the maximum value of the ratio between the torus and bolometric AGN luminosity ( $R_{\text{max}}$ ) to 1.3 for unobscured objects and  $R_{\text{max}} = 1$  for obscured AGN. In the following, we will use the dust covering factors obtained from Equations (2) and (3). We also tested the scenario in which the torus and disk are misaligned (with  $\tau_{9.7} = 5$ ), in which case the  $R_{\text{max}}$  for unobscured objects was set to 1.5 and 1.6 for an inclination of the disk with respect to the torus of  $15^\circ$  and  $30^\circ$ , respectively. We found that this does not significantly affect any of the results reported here.

The median dust covering factors obtained using the approach described above are  $0.50 \pm 0.01$  and  $0.41 \pm 0.02$  for  $\kappa_{2-10} = 20$  and  $\kappa_{2-10} = \kappa(\lambda_{\text{Edd}})$ , respectively. Interestingly, as observed in Ichikawa et al. (2019), these values are significantly lower than the covering factor obtained by X-ray observations for the same sample ( $\sim 70\% \pm 2\%$ ; Ricci et al. 2015, 2017a). This difference could be associated with obscuration from the broad line region (e.g., Davies et al. 2015; Ichikawa et al. 2019) or from dust-free gas associated with outflows produced by the AGN. In Figure 1, we show the dust covering factor of BASS AGN versus the column density inferred by X-ray observations by considering fixed bolometric corrections (blue circles) or Eddington ratio–dependent bolometric corrections (red diamonds). In both cases, the dust covering factor of the obscuring material in an unobscured AGN is  $\sim 1.5$ – $2$  times lower than for an obscured AGN. This is in agreement with previous studies carried out by applying a torus model to the IR emission of nearby AGN (e.g., Ramos Almeida et al. 2011). As proposed by Elitzur (2012), this could be explained simply by the fact that AGN in which the covering factor of the obscuring material is large are more likely to be observed as obscured/type 2 due to the larger fraction of obscured lines of sight.

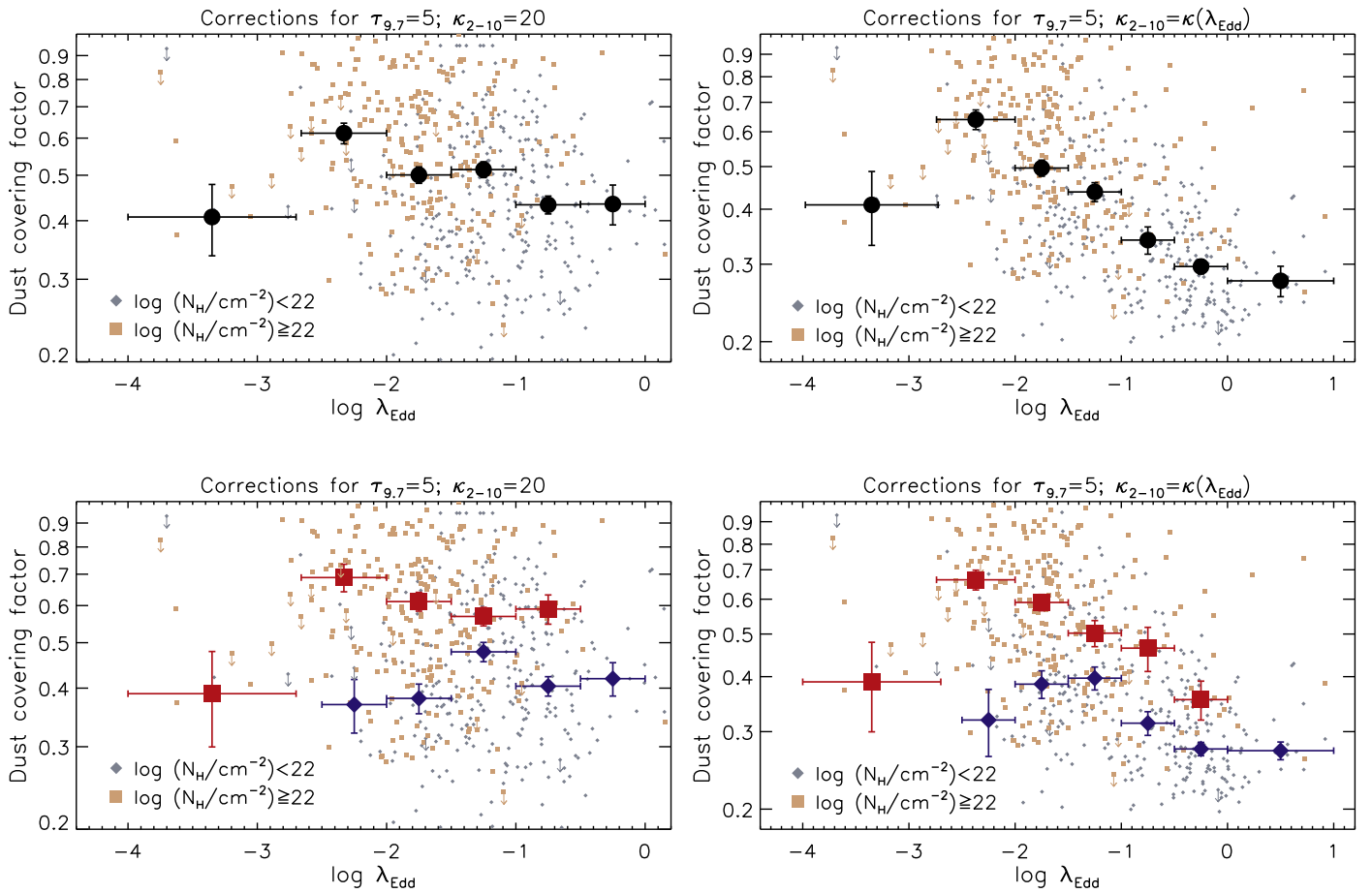
### 3.1. The Dependence of the Covering Factor on the Eddington Ratio

In Figure 2, we illustrate the dust covering factor versus the Eddington ratio for the sources of our sample. This was done



**Figure 1.** Median dust covering factor (see Section 3 and Equations (2) and (3)) vs. column density for the sources of our sample. The bolometric luminosity was estimated by using fixed 2–10 keV bolometric corrections ( $\kappa_{2-10} = 20$ ; blue circles) or the Eddington ratio–dependent corrections of Vasudevan & Fabian (2007; red diamonds). The dust covering factors were calculated assuming an optical depth at  $9.7 \mu\text{m}$  of  $\tau_{9.7} = 5$  and Equations (2) and (3).

considering  $\kappa_{2-10} = 20$  (left panels) and  $\kappa_{2-10} = \kappa(\lambda_{\text{Edd}})$  (right panels). In the top panels, we show the median values of the dust covering factor for the whole sample (large black circles), while in the bottom panels, we illustrate the median values for obscured (large red squares) and unobscured (large blue diamonds) AGN. The medians were calculated considering the upper limits, as outlined in Section 2. In both cases, we find a decrease of the covering factor with the Eddington ratio for AGN with  $\log \lambda_{\text{Edd}} > -3$ , which is steeper when considering the  $\lambda_{\text{Edd}}$ -dependent bolometric corrections of Vasudevan & Fabian (2007). The decrease starts at  $\lambda_{\text{Edd}} \sim 10^{-2}$ , similar to what was observed for the covering factor inferred from the fraction of obscured sources (Ricci et al. 2017a, 2022a). The bottom figures show that obscured AGN tend to have larger covering factors than unobscured AGN, as discussed in Section 3, regardless of their Eddington ratio. When assuming a fixed bolometric correction ( $\kappa_{2-10} = 20$ ), the relation between the dust covering factor and  $\lambda_{\text{Edd}}$  for all AGN is mostly driven by the difference in covering factor between obscured and unobscured AGN and the fact that unobscured AGN are mostly found at higher Eddington ratios (Ricci et al. 2017a). On the other hand, when assuming  $\lambda_{\text{Edd}}$ -dependent bolometric corrections, one can also observe a clear decrease of the dust covering factor with  $\lambda_{\text{Edd}}$  for obscured and unobscured AGN. It should be noted that there is an inherent dependence on the choice of bolometric correction in the values of the covering factor, since they are a function of the ratio between the IR AGN luminosity and the bolometric luminosity. However, a recent study focused on a sample of  $\sim 250$  unobscured BASS AGN with simultaneous X-ray and optical/UV observations, has shown that the Eddington ratio is the main driver of the bolometric corrections (K. K. Gupta et al. 2024, in preparation). To ensure the robustness of our results, we tested two additional bolometric corrections: the luminosity–dependent bolometric corrections from Lusso et al. (2012) and the more recent formulation of the Eddington ratio–dependent bolometric corrections from K. K. Gupta et al. (2024, in preparation). In both cases, we recover trends very similar to those presented here by assuming the bolometric corrections of Vasudevan & Fabian (2007), with two differences: (i) a flatter decrease with  $\lambda_{\text{Edd}}$  for the obscured AGN population when



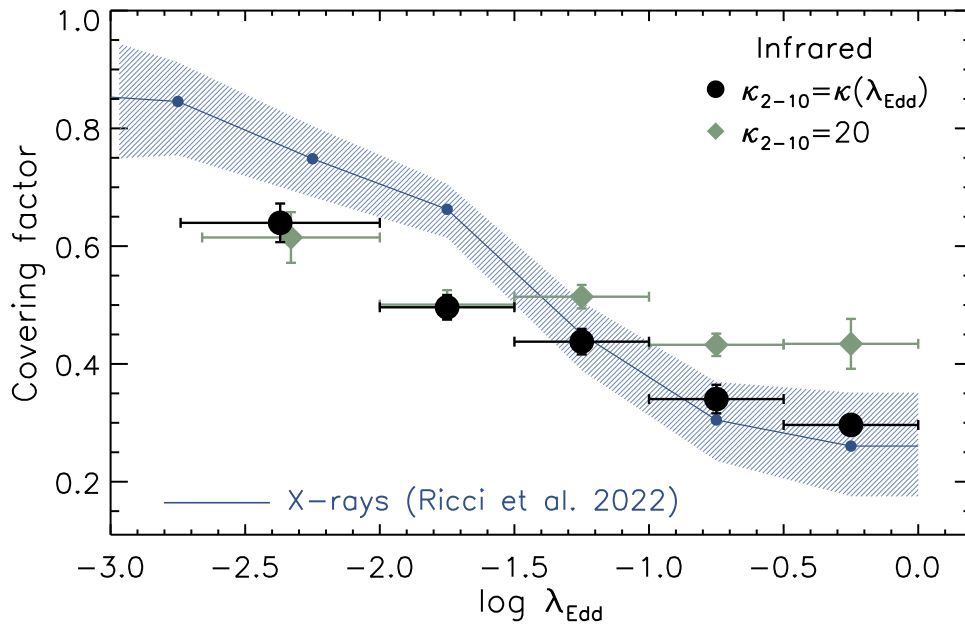
**Figure 2.** Dust covering factor (see Section 3 and Equations (2) and (3)) vs. Eddington ratio for the sources of our sample. The large points in the plots show the median values for the whole population (black circles; top panels) and for unobscured and obscured AGN (blue diamonds and red squares, respectively; bottom panels). The left panels show the case in which the bolometric luminosity is estimated by using a fixed 2–10 keV bolometric correction ( $\kappa_{2-10} = 20$ ), while in the right panels, the bolometric luminosity was estimated by using the Eddington ratio–dependent corrections of Vasudevan & Fabian (2007). The dust covering factors were calculated assuming an optical depth at  $9.7 \mu\text{m}$  of  $\tau_{9.7} = 5$  and Equations (2) and (3).

considering the bolometric corrections from Lusso et al. (2012) and (ii) slightly higher covering factors when using the Gupta et al. (2023, in preparation) bolometric corrections ( $\Delta\text{CF} \sim 0.1$ ). Similar to what we found using  $f_{\text{obs}}$  (Ricci et al. 2017a), and regardless of the choice of the bolometric correction, we see a decrease in the covering factor at low Eddington ratios, which could be associated with an evolutionary sequence of AGN in the  $N_{\text{H}}-\lambda_{\text{Edd}}$  plane (Ricci et al. 2022a; see Section 3.3).

In Ricci et al. (2017a, 2022a), we have shown that the main driver of the covering factor of the Compton-thin obscuring material is the Eddington ratio, and that above the effective Eddington limit for dusty gas ( $\lambda_{\text{Edd}}^{\text{eff}}$ ) with  $N_{\text{H}} \simeq 10^{22} \text{ cm}^{-2}$  ( $\lambda_{\text{Edd}}^{\text{eff}}(10^{22} \text{ cm}^{-2}) \simeq 0.02$ ; see Fabian et al. 2006, 2008, 2009; Arakawa et al. 2022), most AGN are unobscured. The effective Eddington limit is given by the ratio between the Thomson cross section ( $\sigma_{\text{T}}$ ) and the effective cross section of the interaction ( $\sigma_{\text{i}}$ ), i.e.,  $\lambda_{\text{Edd}}^{\text{eff}} = \sigma_{\text{T}}/\sigma_{\text{i}}$ . The value of  $\sigma_{\text{i}}$  depends on the physical properties of the material and is typically  $\sigma_{\text{i}} \gg \sigma_{\text{T}}$ , which implies that  $\lambda_{\text{Edd}}^{\text{eff}} < 1$ . For  $\lambda_{\text{Edd}} \geq \lambda_{\text{Edd}}^{\text{eff}}(N_{\text{H}})$ , the obscuring material is expected to be expelled by radiation pressure, and dusty outflows would be expected to populate the polar region of the system (see Section 3.2). Results consistent with those reported in Ricci et al. (2017a) were also obtained using the ratio between the Eddington ratio distribution

functions of obscured and unobscured Swift/BAT AGN (Ananna et al. 2022a, 2022b) and using the results of broadband X-ray spectroscopy (e.g., Zhao et al. 2020; see also Ogawa et al. 2021) after fixing the inclination angle with respect to the torus to the value obtained from careful modeling of the narrow-line region (Fischer et al. 2013).

In Figure 3, we illustrate the dust covering factors versus  $\lambda_{\text{Edd}}$  obtained in the IR (black circles and green diamonds) together with the covering factor obtained in the X-ray by the recent study of Ricci et al. (2022a; blue line). There is generally a rather good agreement between the values obtained in the IR (for dusty gas) and X-ray (for dust-free and dusty gas). The slightly less steep trend observed in the IR might be ascribed to the fact that, as one moves toward higher  $\lambda_{\text{Edd}}$ , the dust expelled by radiation pressure would still contribute to the IR emission in the form of a polar component (see also García-Bernete et al. 2019; Toba et al. 2021). The relation between the covering factor and  $\lambda_{\text{Edd}}$  implies that, in addition to the inclination angle ( $\theta_{\text{i}}$ ), the observational classification of AGN into obscured and unobscured is driven by the Eddington ratio, in what was defined as the radiation-regulated unification model (Ricci et al. 2017a). If the filling factor of the obscuring clouds is large, the half-opening angle of the torus for a given value of  $\lambda_{\text{Edd}}$  can be deduced from  $\theta_{\text{OA}}(\lambda_{\text{Edd}}) = \cos^{-1}[f_{\text{obs}}^*(\lambda_{\text{Edd}})]$ , where  $f_{\text{obs}}^*$  is the fraction of all obscured



**Figure 3.** Covering factor of dust vs. Eddington ratio for the sources of our samples considering the Eddington ratio–dependent corrections of Vasudevan & Fabian (2007; black circles) and fixed 2–10 keV bolometric corrections ( $\kappa_{2-10} = 20$ ; green diamonds). The solid blue line shows the covering factor of gas inferred from the fraction of obscured sources (Ricci et al. 2022a, assuming  $\kappa_{2-10} = 20$ ; see Ricci et al. 2017a for a discussion on how bolometric corrections affect the  $f_{\text{obs}} - \lambda_{\text{Edd}}$  trend), while the hatched area represents the  $1\sigma$  uncertainty. The dust covering factors were calculated assuming an optical depth at  $9.7 \mu\text{m}$  of  $\tau_{9.7} = 5$  and Equations (2) and (3).

sources (i.e., both Compton-thin and Compton-thick). In this scheme, a source will be unobscured if the inclination angle is smaller than the half-opening angle of the torus ( $\theta_i < \theta_{\text{OA}}(\lambda_{\text{Edd}})$ ), while it will be obscured if  $\theta_i > \theta_{\text{OA}}(\lambda_{\text{Edd}})$ .

### 3.2. Dusty Outflows and Polar Dust

Over the past few years, interferometric studies (Jaffe et al. 2004; Wittkowski et al. 2004; Tristram et al. 2007; Raban et al. 2009; Hönig et al. 2012, 2013; Burtscher et al. 2013; López-Gonzaga et al. 2014; Tristram et al. 2014; López-Gonzaga et al. 2016; Gámez Rosas et al. 2022; Isbell et al. 2022) and high spatial resolution observations carried out by 8–10 m telescopes (Asmus et al. 2016; García-Bernete et al. 2016) have shown that a significant fraction of the mid-IR emission of AGN is elongated in the polar direction, and models including a disk and a wind can reproduce the near-to-mid-IR properties of local AGN (Hönig & Kishimoto 2017). The elongated mid-IR emission, which is thought to originate in a hollow cone (e.g., Stalevski et al. 2017, 2019), could be related to dusty outflows arising at  $\lambda_{\text{Edd}} \geq \lambda_{\text{Edd}}^{\text{eff}}(N_{\text{H}})$  (e.g., Hönig et al. 2012; Tazaki & Ichikawa 2020; Venanzi et al. 2020). Such outflows could also be associated with larger-scale winds observed in AGN (e.g., Kakkad et al. 2016; Rojas et al. 2020; Musiimenta et al. 2023; Stacey et al. 2022).

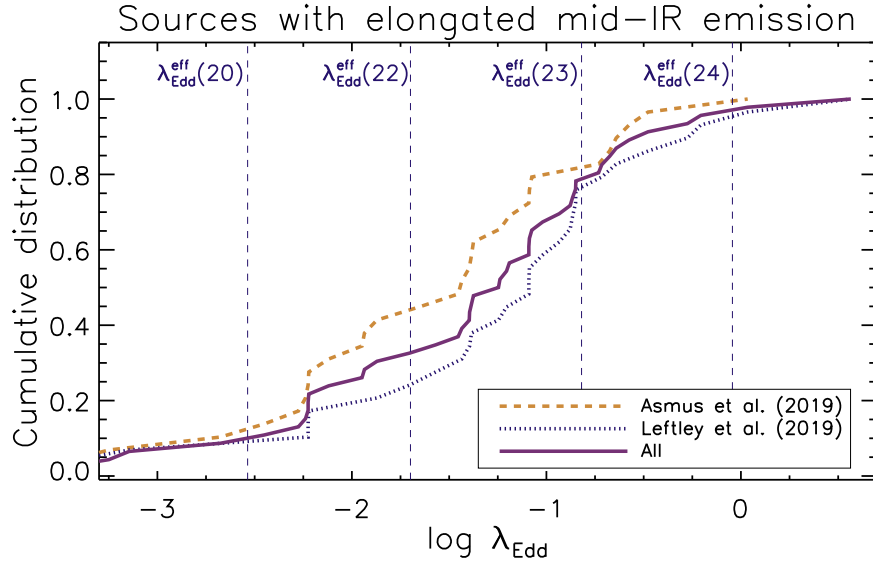
Consistent with the idea that radiation pressure is responsible for the extended IR emission in AGN, the Eddington ratio of the objects currently known to show polar mid-IR emission is typically rather high. Some of the sources where polar dust was observed, such as Circinus (Tristram et al. 2014), NGC 424 (Hönig et al. 2012), and NGC 1068 (López-Gonzaga et al. 2014), are among the obscured AGN with the highest Eddington ratio in our sample (see also Leftley et al. 2019), and several of them lie in the forbidden region of the  $N_{\text{H}} - \lambda_{\text{Edd}}$  diagram. Indeed, Alonso-Herrero et al. (2021) found that AGN with polar mid-IR emission show intermediate column

densities [ $\log(N_{\text{H}}/\text{cm}^{-2}) \sim 22.5\text{--}23$ ] and Eddington ratios ( $\log \lambda_{\text{Edd}} \sim -1.75$  to  $-1$ ). García-Bernete et al. (2022) fitted the IR spectra of nearby AGN from the Swift/BAT sample and found that AGN that are best reproduced by models that include a polar dust component typically have  $\log \lambda_{\text{Edd}} \gtrsim -2.5$  (see also González-Martín et al. 2019). Yamada et al. (2023) showed, for a sample of nearby AGN undergoing mergers, that the contribution of the polar component to the IR AGN luminosity increases for  $\log \lambda_{\text{Edd}} \gtrsim -3$  (see their Figure 21). However, it should be noted that the forbidden region is defined for the line-of-sight column density  $N_{\text{H}}$ , so even sources accreting at  $\lambda_{\text{Edd}} < \lambda_{\text{Edd}}^{\text{eff}}(N_{\text{H}})$  might be in the process of expelling some material if, for some inclination angles, the clouds surrounding the SMBH have column densities ( $N_{\text{H}}(\theta_i)$ ) lower than the value inferred for the line of sight and such that  $\lambda_{\text{Edd}} \geq \lambda_{\text{Edd}}^{\text{eff}}[N_{\text{H}}(\theta_i)]$ .

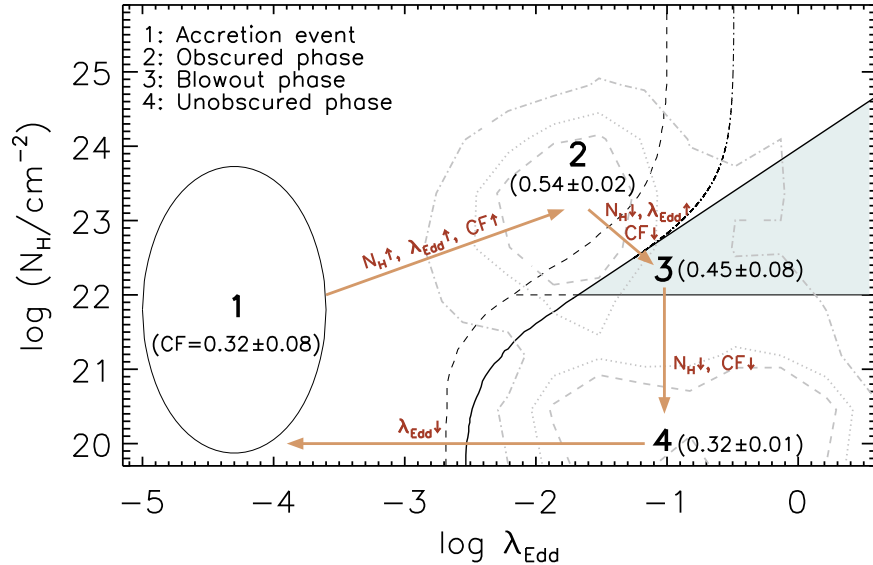
In Figure 4, we illustrate the cumulative Eddington ratio distribution of sources showing mid-IR polar emission from interferometric (Leftley et al. 2019; dotted blue line) and high-resolution single-dish (Asmus 2019; dashed orange line) observations, most of which are part of our Swift/BAT-selected sample. Interestingly, all of the sources showing elongated mid-IR emission are accreting above the Eddington limit for dusty gas with  $N_{\text{H}} = 10^{20} \text{ cm}^{-2}$ , and more than half of them ( $61\% \pm 10\%$ ) are at  $\lambda_{\text{Edd}} \geq \lambda_{\text{Edd}}^{\text{eff}}(10^{22} \text{ cm}^{-2})$ . A possible caveat of these studies is that we might preferentially detect extended IR emission in AGN with higher luminosities and Eddington ratios because of the stronger contrasts with respect to the host galaxy, whose emission could hide extended IR emission at low accretion rates.

### 3.3. Radiation-regulated SMBH Growth

As argued by Ricci et al. (2017a), the radiation-regulated unification model could be dynamic, with AGN moving in the  $N_{\text{H}} - \lambda$  diagram during their lifetime (see also Jun et al. 2021;



**Figure 4.** Cumulative Eddington ratio distribution of sources showing polar mid-IR emission. Cumulative distribution of  $\lambda_{\text{Edd}}$  for sources showing elongated mid-IR emission from interferometric (Leftley et al. 2019; dotted blue line) and high-resolution noninterferometric (Asmus 2019; dashed orange line) observations. The solid line shows the total cumulative distribution. The dashed vertical lines represent the effective Eddington limit for dusty gas with  $N_{\text{H}} = 10^{20} \text{ cm}^{-2}$  [ $\lambda_{\text{Edd}}^{\text{eff}}(20)$ ],  $N_{\text{H}} = 10^{22} \text{ cm}^{-2}$  [ $\lambda_{\text{Edd}}^{\text{eff}}(22)$ ],  $N_{\text{H}} = 10^{23} \text{ cm}^{-2}$  [ $\lambda_{\text{Edd}}^{\text{eff}}(23)$ ], and  $N_{\text{H}} = 10^{24} \text{ cm}^{-2}$  [ $\lambda_{\text{Edd}}^{\text{eff}}(24)$ ] for dust grain abundance consistent with the ISM.



**Figure 5.** Schematic of radiation-regulated growth of SMBHs together with the median covering factors of dusty gas at different stages (see Section 3.3). The effective Eddington limit for dusty gas reported in Fabian et al. (2009) is shown with the black solid lines, while the blowout region is the green area. The plot also shows the effective Eddington limit when including IR radiation trapping (Ishibashi et al. 2018), adapted to the values of Fabian et al. (2009), similar to what was done by Lansbury et al. (2020; dashed-dotted lines). The effective Eddington limit for dusty gas reported by Ishibashi et al. (2018) is shown by the dashed line. The assumed maximum contribution to  $N_{\text{H}}$  of gas from the host galaxy is illustrated by the horizontal line at  $\log(N_{\text{H}}/\text{cm}^{-2}) = 22$ . The number density contours in the  $-3 \leq \log \lambda_{\text{Edd}} \leq 1$  range are shown by the gray dashed (50%), dotted (68%), and dotted-dashed (90%) lines. The bolometric corrections of Vasudevan & Fabian (2007) were used for both CF and  $\lambda_{\text{Edd}}$ .

Toba et al. 2022). Ricci et al. (2022a) showed that the breaks observed in both the Eddington ratio distribution function and the luminosity function (Ananna et al. 2022b) correspond to the  $\lambda_{\text{Edd}}$  and  $L_{14-150 \text{ keV}}$  at which AGN transition from having most of their sky covered by absorbing material to having most of their sky devoid of obscuring material (see Figure 4 of Ricci et al. 2022a). This implies that the majority of the SMBH growth at  $z \sim 0$  happens when most of the AGN is covered by gas and dust, and that AGN accreting above the Eddington limit for dusty gas are rarer. Ricci et al. (2022a) proposed that this could be related to the lower amount of material available to feed the SMBH when the AGN is accreting very rapidly due

to the depletion of the gas reservoir caused by radiation pressure, and that AGN could move in the  $N_{\text{H}}-\lambda_{\text{Edd}}$  plane during their life cycle (see Figure 5). In this picture, SMBHs start their growth phase at low  $\lambda_{\text{Edd}}$  in a mostly unobscured phase (stage 1). As the fuel moves toward the SMBH,  $\lambda_{\text{Edd}}$ ,  $N_{\text{H}}$ , and the covering factor would gradually increase, leading the source to be preferentially observed as obscured by observers with random inclination angles (stage 2). Once  $\lambda_{\text{Edd}} \gtrsim \lambda_{\text{Edd}}^{\text{eff}}$ , the AGN would start expelling the obscuring material (stage 3), which would lead to a decrease in both its covering factor and typical  $N_{\text{H}}$ , and the source would be preferentially observed as an unobscured AGN (stage 4). This last phase is expected to be

rather short, lasting  $\sim 3\text{--}30$  Myr (Ananna et al. 2022a; assuming an AGN lifetime of  $\sim 10^7\text{--}10^8$  yr). Once the AGN accretes the rest of the material, it will move toward low Eddington ratios again (stage 1). Interestingly, studying ALMA observations of 19 nearby AGN, García-Burillo et al. (2021) recently found a tentative decline of the average molecular gas surface density and  $\text{H}_2$  column density for increasing Eddington ratios. They interpreted this, and the presence of molecular deficits on nuclear scales, as a signature of AGN feedback and possibly an evolutionary sequence of AGN for increasing luminosities and Eddington ratios, similar to that proposed by Ricci et al. (2017a, 2022a).

Using the dust covering factor we estimated from IR luminosities, we can test this model and, in particular, check whether the typical covering factors change from stage 1 to stage 4. To do this, we used the bolometric corrections of Vasudevan & Fabian (2007) and divided the  $N_{\text{H}}\text{--}\lambda$  into different regions. For stage 1, we considered all objects with  $\log \lambda_{\text{Edd}} \leq -3.5$ , while for stage 2, we used all obscured AGN with  $-3.5 \leq \log \lambda_{\text{Edd}} \leq \log \lambda_{\text{Edd}}^{\text{eff}}(N_{\text{H}})$ , using the original definition of  $\lambda_{\text{Edd}}^{\text{eff}}(N_{\text{H}})$  (Fabian et al. 2009; black solid curve in Figure 5). For stage 3, we considered all obscured AGN in the blowout region (green area in Figure 5),  $\log \lambda_{\text{Edd}} \geq \log \lambda_{\text{Edd}}^{\text{eff}}(N_{\text{H}})$ . Finally, for stage 4, we used all unobscured AGN with  $\log \lambda_{\text{Edd}} > -1.75$  (i.e., a value corresponding to  $\sim \log \lambda_{\text{Edd}}^{\text{eff}}(10^{22} \text{ cm}^{-2})$ ). The median covering factors we obtain agree well with the expected general trends; it is the lowest in stage 1 ( $0.32 \pm 0.08$ ), increases by a factor of 2 in stage 2 ( $0.54 \pm 0.02$ ), and then decreases, likely due to the effect of radiation pressure, in stage 3 ( $0.45 \pm 0.08$ ) and stage 4 ( $0.32 \pm 0.01$ ). It should be stressed that in stage 1, the covering factors could actually be lower than what was inferred here due to our AGN selection, which is missing AGN that accrete at very low Eddington ratios ( $\log \lambda_{\text{Edd}} < -4$ ). In fact, besides showing little absorption (see also She et al. 2018), AGN accreting at very low  $\lambda_{\text{Edd}}$  also typically display faint reflection features (e.g., Ptak et al. 2004; Bianchi et al. 2017; Diaz et al. 2020, 2023; Jana et al. 2023; see Ho 2008 for a review of the subject).

#### 4. Summary and Conclusion

In this paper, we studied a sample of 549 nearby nonblazar hard X-ray selected AGN (Section 2) to investigate the relation of the covering factor of dust around SMBHs and the Eddington ratio. We used the ratio of IR and bolometric AGN luminosity as a proxy of the covering factor of the circumnuclear dusty gas, considering the corrections of Stalevski et al. (2016; Section 3). In the following, we summarize our main findings.

1. We find that obscured AGN typically have a higher covering factor than their unobscured counterparts (Figure 1), consistent with previous studies of the IR SEDs of nearby AGN (e.g., Ramos Almeida et al. 2011). This is in agreement with the idea that AGN with large covering factors of obscuring material are more likely to be observed as obscured/type 2 due to the larger fraction of obscured lines of sight (Elitzur 2012).
2. The dust covering factor shows a decrease with the Eddington ratio (Section 3.1) similar to that observed in the X-ray band (Ricci et al. 2017a, 2022a; Figures 2 and 3), which was attributed to the effect of radiation pressure

on the dusty gas. The relation between the covering factor and  $\lambda_{\text{Edd}}$  implies that, besides the inclination angle, the observational classification of AGN into obscured and unobscured is driven by the Eddington ratio (radiation-regulated unification model; Ricci et al. 2017a).

3. The obscuring material expelled by radiation pressure would be expected to populate the polar region of the system (see Section 3.2) and could be responsible for the extended mid-IR emission observed in a growing number of AGN (e.g., Hönig et al. 2012; Venanzi et al. 2020). In agreement with this, we find that all of the sources showing elongated mid-IR emission are accreting with Eddington ratios above the Eddington limit for dusty gas with  $N_{\text{H}} = 10^{20} \text{ cm}^{-2}$ , and more than half of them are above the Eddington limit for dusty gas with  $N_{\text{H}} = 10^{22} \text{ cm}^{-2}$  (Figure 4).
4. The median covering factors obtained for AGN located in different regions of the  $N_{\text{H}}\text{--}\lambda_{\text{Edd}}$  plane are consistent with what would be expected if the growth of SMBHs were regulated by radiation (Ricci et al. 2022a; Section 3.3) and AGN moved through the  $N_{\text{H}}\text{--}\lambda_{\text{Edd}}$  plane during their lifetime (Figure 5).

#### Acknowledgments















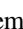

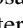

We thank the referee for comments, which helped us improve the quality of our manuscript. We acknowledge support from the National Science Foundation of China 11721303, 11991052, 12011540375, and 12233001 (L.H.); the National Key R&D Program of China 2022YFF0503401 (L.H.); the China Manned Space Project CMS-CSST-2021-A04 and CMS-CSST-2021-A06 (L.H.); Fondecyt Regular grant 1230345 (C.R.) and ANID BASAL project FB210003 (C.R., F.E.B., E.T.); NASA through ADAP award NNH16CT03C (M.K.); the Israel Science Foundation through grant No. 1849/19 (B.T.); the European Research Council (ERC) under the European Union’s Horizon 2020 research and innovation program through grant agreement No. 950533 (B. T.); Fondecyt fellowship No. 3220516 (M.T.); the Korea Astronomy and Space Science Institute under the R&D program (project No. 2022-1-868-04) supervised by the Ministry of Science and ICT (K.O.); the National Research Foundation of Korea (NRF-2020R1C1C1005462) (K.O.); Fondecyt Postdoctorado 3210157 (A.R.); RIN MIUR 2017 project “Black Hole winds and the Baryon Life Cycle of Galaxies: the stone-guest at the galaxy evolution supper,” contract 2017PH3WAT (F.R.); the ANID—Millennium Science Initiative Program—ICN12\_009 (F.E.B.); CATA-Basal—ACE210002 (F.E.B., E.T.); FONDECYT Regular—1190818 (F.E.B., E.T.) and 1200495 (F.E.B., E.T.); Núcleo Milenio NCN\_058 (E.T.); the Science Fund of the Republic of Serbia, PROMIS 6060916, BOWIE; and the Ministry of Education, Science and Technological Development of the Republic of Serbia through contract No. 451-03-9/2023-14/200002 (M.S.). This work made use of data from the NASA/IPAC Infrared Science Archive and NASA/IPAC Extragalactic Database (NED), which are operated by the Jet Propulsion Laboratory, California Institute of Technology, under contract with the National Aeronautics and Space Administration. This research has made use of data and/or software provided by the High Energy Astrophysics Science Archive Research Center (HEASARC), which is a service of the Astrophysics Science



Division at NASA/GSFC and the High Energy Astrophysics  
Division of the Smithsonian Astrophysical Observatory.

Facilities: Swift, WISE, IRAS, Akari, Spitzer

### ORCID iDs

C. Ricci  <https://orcid.org/0000-0001-5231-2645>  
 K. Ichikawa  <https://orcid.org/0000-0002-4377-903X>  
 M. Stalevski  <https://orcid.org/0000-0001-5146-8330>  
 T. Kawamuro  <https://orcid.org/0000-0002-6808-2052>  
 S. Yamada  <https://orcid.org/0000-0002-9754-3081>  
 Y. Ueda  <https://orcid.org/0000-0001-7821-6715>  
 R. Mushotzky  <https://orcid.org/0000-0002-7962-5446>  
 G. C. Privon  <https://orcid.org/0000-0003-3474-1125>  
 M. J. Koss  <https://orcid.org/0000-0002-7998-9581>  
 B. Trakhtenbrot  <https://orcid.org/0000-0002-3683-7297>  
 A. C. Fabian  <https://orcid.org/0000-0002-9378-4072>  
 L. C. Ho  <https://orcid.org/0000-0001-6947-5846>  
 F. E. Bauer  <https://orcid.org/0000-0002-8686-8737>  
 C. S. Chang  <https://orcid.org/0000-0001-9910-3234>  
 K. K. Gupta  <https://orcid.org/0009-0007-9018-1077>  
 K. Oh  <https://orcid.org/0000-0002-5037-951X>  
 M. Powell  <https://orcid.org/0000-0003-2284-8603>  
 R. W. Pfeifle  <https://orcid.org/0000-0001-8640-8522>  
 A. Rojas  <https://orcid.org/0000-0003-0006-8681>  
 F. Ricci  <https://orcid.org/0000-0001-5742-5980>  
 M. J. Temple  <https://orcid.org/0000-0001-8433-550X>  
 Y. Toba  <https://orcid.org/0000-0002-3531-7863>  
 A. Tortosa  <https://orcid.org/0000-0003-3450-6483>  
 E. Treister  <https://orcid.org/0000-0001-7568-6412>  
 D. Stern  <https://orcid.org/0000-0003-2686-9241>  
 C. M. Urry  <https://orcid.org/0000-0002-0745-9792>

### References

- Alonso-Herrero, A., Ramos Almeida, C., Mason, R., et al. 2011, *ApJ*, 736, 82  
 Alonso-Herrero, A., García-Burillo, S., Hönig, S. F., et al. 2021, *A&A*, 652, A99  
 Ananna, T. T., Urry, C. M., Ricci, C., et al. 2022a, *ApJL*, 939, L13  
 Ananna, T. T., Weigel, A. K., Trakhtenbrot, B., et al. 2022b, *ApJS*, 261, 9  
 Andonie, C., Ricci, C., Paltani, S., et al. 2022, *MNRAS*, 511, 5768  
 Antonucci, R. 1993, *ARA&A*, 31, 473  
 Arakawa, N., Fabian, A. C., Ferland, G. J., & Ishibashi, W. 2022, *MNRAS*, 517, 5069  
 Asmus, D. 2019, *MNRAS*, 489, 2177  
 Asmus, D., Hönig, S. F., & Gandhi, P. 2016, *ApJ*, 822, 109  
 Asmus, D., Hönig, S. F., Gandhi, P., Smette, A., & Duschl, W. J. 2014, *MNRAS*, 439, 1648  
 Assef, R. J., Stern, D., Kochanek, C. S., et al. 2013, *ApJ*, 772, 26  
 Awaki, H., Koyama, K., Inoue, H., & Halpern, J. P. 1991, *PASJ*, 43, 195  
 Baloković, M., Brightman, M., Harrison, F. A., et al. 2018, *ApJ*, 854, 42  
 Barthelmy, S. D., Barbier, L. M., Cummings, J. R., et al. 2005, *SSRv*, 120, 143  
 Baumgartner, W. H., Tueller, J., Markwardt, C. B., et al. 2013, *ApJS*, 207, 19  
 Beckmann, V., Soldi, S., Ricci, C., et al. 2009, *A&A*, 505, 417  
 Bianchi, S., Guainazzi, M., Matt, G., & Fonseca Bonilla, N. 2007, *A&A*, 467, L19  
 Bianchi, S., Marinucci, A., Matt, G., et al. 2017, *MNRAS*, 468, 2740  
 Boorman, P. G., Gandhi, P., Baloković, M., et al. 2018, *MNRAS*, 477, 3775  
 Brightman, M., Baloković, M., Stern, D., et al. 2015, *ApJ*, 805, 41  
 Brightman, M., & Nandra, K. 2011, *MNRAS*, 413, 1206  
 Buchner, J., & Bauer, F. E. 2017, *MNRAS*, 465, 4348  
 Buchner, J., Brightman, M., Baloković, M., et al. 2021, *A&A*, 651, A58  
 Buchner, J., Georgakakis, A., Nandra, K., et al. 2015, *ApJ*, 802, 89  
 Burlon, D., Ajello, M., Greiner, J., et al. 2011, *ApJ*, 728, 58  
 Burtscher, L., Meisenheimer, K., Tristram, K. R. W., et al. 2013, *A&A*, 558, A149  
 Campitiello, S., Ghisellini, G., Sbarrato, T., & Calderone, G. 2018, *A&A*, 612, A59  
 Davies, R. I., Burtscher, L., Rosario, D., et al. 2015, *ApJ*, 806, 127  
 Della Ceca, R., Caccianiga, A., Severgnini, P., et al. 2008, *A&A*, 487, 119  
 Diaz, Y., Arévalo, P., Hernández-García, L., et al. 2020, *MNRAS*, 496, 5399  
 Diaz, Y., Hernández-García, L., Arévalo, P., et al. 2023, *A&A*, 669, A114  
 Elitzur, M. 2008, *NewAR*, 52, 274  
 Elitzur, M. 2012, *ApJL*, 747, L33  
 Ezhikode, S. H., Gandhi, P., Done, C., et al. 2017, *MNRAS*, 472, 3492  
 Fabian, A. C., Celotti, A., & Erlund, M. C. 2006, *MNRAS*, 373, L16  
 Fabian, A. C., Vasudevan, R. V., & Gandhi, P. 2008, *MNRAS*, 385, L43  
 Fabian, A. C., Vasudevan, R. V., Mushotzky, R. F., Winter, L. M., & Reynolds, C. S. 2009, *MNRAS*, 394, L89  
 Feigelson, E. D., & Nelson, P. I. 1985, *ApJ*, 293, 192  
 Fischer, T. C., Crenshaw, D. M., Kraemer, S. B., & Schmitt, H. R. 2013, *ApJS*, 209, 1  
 Gámez Rosas, V., Isbell, J. W., Jaffe, W., et al. 2022, *Natur*, 602, 403  
 Gandhi, P., Horst, H., Smette, A., et al. 2009, *A&A*, 502, 457  
 García-Bernete, I., González-Martín, O., Ramos Almeida, C., et al. 2022, *A&A*, 667, A140  
 García-Bernete, I., Ramos Almeida, C., Acosta-Pulido, J. A., et al. 2016, *MNRAS*, 463, 3531  
 García-Bernete, I., Ramos Almeida, C., Alonso-Herrero, A., et al. 2019, *MNRAS*, 486, 4917  
 García-Burillo, S., Alonso-Herrero, A., Ramos Almeida, C., et al. 2021, *A&A*, 652, A98  
 García-Burillo, S., Combes, F., Ramos Almeida, C., et al. 2019, *A&A*, 632, A61  
 Gehrels, N., Chincarini, G., Giommi, P., et al. 2004, *ApJ*, 611, 1005  
 Georgantopoulos, I., & Georgakakis, A. 2005, *MNRAS*, 358, 131  
 González-Martín, O., Masegosa, J., García-Bernete, I., et al. 2019, *ApJ*, 884, 10  
 Granato, G. L., & Danese, L. 1994, *MNRAS*, 268, 235  
 Harrison, C. M. 2017, *NatAs*, 1, 0165  
 Hasinger, G. 2008, *A&A*, 490, 905  
 Hickox, R. C., & Alexander, D. M. 2018, *ARA&A*, 56, 625  
 Ho, L. C. 2008, *ARA&A*, 46, 475  
 Hönig, S. F., Beckert, T., Ohnaka, K., & Weigelt, G. 2006, *A&A*, 452, 459  
 Hönig, S. F., & Kishimoto, M. 2010, *A&A*, 523, A27  
 Hönig, S. F., & Kishimoto, M. 2017, *ApJL*, 838, L20  
 Hönig, S. F., Kishimoto, M., Antonucci, R., et al. 2012, *ApJ*, 755, 149  
 Hönig, S. F., Kishimoto, M., Gandhi, P., et al. 2010, *A&A*, 515, A23  
 Hönig, S. F., Kishimoto, M., Tristram, K. R. W., et al. 2013, *ApJ*, 771, 87  
 Ichikawa, K., Packham, C., Ramos Almeida, C., et al. 2015, *ApJ*, 803, 57  
 Ichikawa, K., Ricci, C., Ueda, Y., et al. 2017, *ApJ*, 835, 74  
 Ichikawa, K., Ricci, C., Ueda, Y., et al. 2019, *ApJ*, 870, 31  
 Imanishi, M., Nguyen, D. D., Wada, K., et al. 2020, *ApJ*, 902, 99  
 Impellizzeri, C. M. V., Gallimore, J. F., Baum, S. A., et al. 2019, *ApJL*, 884, L28  
 Inaba, K., Ueda, Y., Yamada, S., et al. 2022, *ApJ*, 939, 88  
 Isbell, J. W., Meisenheimer, K., Pott, J. U., et al. 2022, *A&A*, 663, A35  
 Ishibashi, W., Fabian, A. C., & Reynolds, C. S. 2019, *MNRAS*, 486, 2210  
 Ishibashi, W., Fabian, A. C., Ricci, C., & Celotti, A. 2018, *MNRAS*, 479, 3335  
 Isobe, T., Feigelson, E. D., & Nelson, P. I. 1986, *ApJ*, 306, 490  
 Iwasawa, K., & Taniguchi, Y. 1993, *ApJL*, 413, L15  
 Jaffe, W., Meisenheimer, K., Röttgering, H. J. A., et al. 2004, *Natur*, 429, 47  
 Jana, A., Chatterjee, A., Chang, H.-K., et al. 2023, *MNRAS*, 524, 4670  
 Jun, H. D., Assef, R. J., Carroll, C. M., et al. 2021, *ApJ*, 906, 21  
 Kakkad, D., Mainieri, V., Padovani, P., et al. 2016, *A&A*, 592, A148  
 Komendy, J., & Ho, L. C. 2013, *ARA&A*, 51, 511  
 Koss, M., Trakhtenbrot, B., Ricci, C., et al. 2017, *ApJ*, 850, 74  
 Koss, M. J., Assef, R., Baloković, M., et al. 2016, *ApJ*, 825, 85  
 Koss, M. J., Ricci, C., Trakhtenbrot, B., et al. 2022b, *ApJS*, 261, 2  
 Koss, M. J., Trakhtenbrot, B., Ricci, C., et al. 2022a, *ApJS*, 261, 1  
 Koss, M. J., Trakhtenbrot, B., Ricci, C., et al. 2022c, *ApJS*, 261, 6  
 Krolik, J. H., & Begelman, M. C. 1988, *ApJ*, 329, 702  
 La Franca, F., Fiore, F., Comastri, A., et al. 2005, *ApJ*, 635, 864  
 Lacy, M., Ridgway, S. E., Sajina, A., et al. 2015, *ApJ*, 802, 102  
 Lansbury, G. B., Banerji, M., Fabian, A. C., & Temple, M. J. 2020, *MNRAS*, 495, 2652  
 Lanz, L., Hickox, R. C., Baloković, M., et al. 2019, *ApJ*, 870, 26  
 Lawrence, A. 1991, *MNRAS*, 252, 586  
 Lawrence, A., & Elvis, M. 1982, *ApJ*, 256, 410  
 Lawrence, A., & Elvis, M. 2010, *ApJ*, 714, 561  
 Leftley, J. H., Hönig, S. F., Asmus, D., et al. 2019, *ApJ*, 886, 55  
 Lightman, A. P., & White, T. R. 1988, *ApJ*, 335, 57  
 Liu, Y., & Li, X. 2014, *ApJ*, 787, 52  
 López-Gonzaga, N., Burtscher, L., Tristram, K. R. W., Meisenheimer, K., & Schartmann, M. 2016, *A&A*, 591, A47  
 López-Gonzaga, N., Jaffe, W., Burtscher, L., Tristram, K. R. W., & Meisenheimer, K. 2014, *A&A*, 565, A71

- Lusso, E., Comastri, A., Simmons, B. D., et al. 2012, *MNRAS*, **425**, 623
- Lusso, E., Hennawi, J. F., Comastri, A., et al. 2013, *ApJ*, **777**, 86
- Maiolino, R., Shemmer, O., Imanishi, M., et al. 2007, *A&A*, **468**, 979
- Mateos, S., Carrera, F. J., Alonso-Herrero, A., et al. 2016, *ApJ*, **819**, 166
- Matt, G., & Iwasawa, K. 2019, *MNRAS*, **482**, 151
- Matt, G., Perola, G. C., & Piro, L. 1991, *A&A*, **247**, 25
- Mejía-Restrepo, J. E., Trakhtenbrot, B., Koss, M. J., et al. 2022, *ApJS*, **261**, 5
- Merloni, A., Bongiorno, A., Brusa, M., et al. 2014, *MNRAS*, **437**, 3550
- Mor, R., Netzer, H., & Elitzur, M. 2009, *ApJ*, **705**, 298
- Mullaney, J. R., Alexander, D. M., Goulding, A. D., & Hickox, R. C. 2011, *MNRAS*, **414**, 1082
- Murphy, K. D., & Yaqoob, T. 2009, *MNRAS*, **397**, 1549
- Musiimenta, B., Brusa, M., Liu, T., et al. 2023, *A&A*, **679**, A84
- Nenkova, M., Sirocky, M. M., Ivezić, Z., & Elitzur, M. 2008a, *ApJ*, **685**, 147
- Nenkova, M., Sirocky, M. M., Nikutta, R., Ivezić, Z., & Elitzur, M. 2008b, *ApJ*, **685**, 160
- Netzer, H. 2015, *ARA&A*, **53**, 365
- Netzer, H., Lani, C., Nordon, R., et al. 2016, *ApJ*, **819**, 123
- Nikutta, R., Elitzur, M., & Lacy, M. 2009, *ApJ*, **707**, 1550
- Ogawa, S., Ueda, Y., Tanimoto, A., & Yamada, S. 2021, *ApJ*, **906**, 84
- Ogawa, S., Ueda, Y., Yamada, S., Tanimoto, A., & Kawaguchi, T. 2019, *ApJ*, **875**, 115
- Oh, K., Yi, S. K., Schawinski, K., et al. 2015, *ApJS*, **219**, 1
- Paltani, S., & Ricci, C. 2017, *A&A*, **607**, A31
- Pösterl, S. 2020, *J. Mach. Learn. Res.*, **21**, 1
- Pounds, K. A., Nandra, K., Stewart, G. C., George, I. M., & Fabian, A. C. 1990, *Natur*, **344**, 132
- Ptak, A., Terashima, Y., Ho, L. C., & Quataert, E. 2004, *ApJ*, **606**, 173
- Raban, D., Jaffe, W., Röttgering, H., Meisenheimer, K., & Tristram, K. R. W. 2009, *MNRAS*, **394**, 1325
- Ramos Almeida, C., Levenson, N. A., Alonso-Herrero, A., et al. 2011, *ApJ*, **731**, 92
- Ramos Almeida, C., & Ricci, C. 2017, *NatAs*, **1**, 679
- Ricci, C., Ananna, T. T., Temple, M. J., et al. 2022a, *ApJ*, **938**, 67
- Ricci, C., & Paltani, S. 2023, *ApJ*, **945**, 55
- Ricci, C., Paltani, S., Awaki, H., et al. 2013, *A&A*, **553**, A29
- Ricci, C., Trakhtenbrot, B., Koss, M. J., et al. 2017a, *Natur*, **549**, 488
- Ricci, C., Trakhtenbrot, B., Koss, M. J., et al. 2017b, *ApJS*, **233**, 17
- Ricci, C., Ueda, Y., Koss, M. J., et al. 2015, *ApJL*, **815**, L13
- Ricci, C., Ueda, Y., Paltani, S., et al. 2014, *MNRAS*, **441**, 3622
- Ricci, F., Treister, E., Bauer, F. E., et al. 2022b, *ApJS*, **261**, 8
- Rojas, A. F., Sani, E., Gavignaud, I., et al. 2020, *MNRAS*, **491**, 5867
- Sazonov, S., Revnivtsev, M., Krivonos, R., Churazov, E., & Sunyaev, R. 2007, *A&A*, **462**, 57
- Schartmann, M., Meisenheimer, K., Camenzind, M., et al. 2008, *A&A*, **482**, 67
- She, R., Ho, L. C., Feng, H., & Cui, C. 2018, *ApJ*, **859**, 152
- Shimizu, T. T., Meléndez, M., Mushotzky, R. F., et al. 2016, *MNRAS*, **456**, 3335
- Siebenmorgen, R., Heymann, F., & Efstathiou, A. 2015, *A&A*, **583**, A120
- Simpson, C. 2005, *MNRAS*, **360**, 565
- Smith, K. L., Koss, M., & Mushotzky, R. F. 2014, *ApJ*, **794**, 112
- Stalevski, M., Asmus, D., & Tristram, K. R. W. 2017, *MNRAS*, **472**, 3854
- Stalevski, M., Fritz, J., Baes, M., Nakos, T., & Popović, L. Č. 2012, *MNRAS*, **420**, 2756
- Stacey, H. R., Costa, T., McKean, J. P., et al. 2022, *MNRAS*, **517**, 3377
- Stalevski, M., Ricci, C., Ueda, Y., et al. 2016, *MNRAS*, **458**, 2288
- Stalevski, M., Tristram, K. R. W., & Asmus, D. 2019, *MNRAS*, **484**, 3334
- Tanimoto, A., Ueda, Y., Odaka, H., et al. 2019, *ApJ*, **877**, 95
- Tanimoto, A., Ueda, Y., Odaka, H., et al. 2020, *ApJ*, **897**, 2
- Tazaki, R., & Ichikawa, K. 2020, *ApJ*, **892**, 149
- Toba, Y., Liu, T., Urrutia, T., et al. 2022, *A&A*, **661**, A15
- Toba, Y., Oyabu, S., Matsuhara, H., et al. 2013, *PASJ*, **65**, 113
- Toba, Y., Oyabu, S., Matsuhara, H., et al. 2014, *ApJ*, **788**, 45
- Toba, Y., Ueda, Y., Gandhi, P., et al. 2021, *ApJ*, **912**, 91
- Treister, E., Krolik, J. H., & Dullemond, C. 2008, *ApJ*, **679**, 140
- Treister, E., & Urry, C. M. 2005, *ApJ*, **630**, 115
- Treister, E., & Urry, C. M. 2006, *ApJL*, **652**, L79
- Tristram, K. R. W., Burtscher, L., Jaffe, W., et al. 2014, *A&A*, **563**, A82
- Tristram, K. R. W., Impellizzeri, C. M. V., Zhang, Z.-Y., et al. 2022, *A&A*, **664**, A142
- Tristram, K. R. W., Meisenheimer, K., Jaffe, W., et al. 2007, *A&A*, **474**, 837
- Tueller, J., Mushotzky, R. F., Barthelmy, S., et al. 2008, *ApJ*, **681**, 113
- Ueda, Y., Akiyama, M., Hasinger, G., Miyaji, T., & Watson, M. G. 2014, *ApJ*, **786**, 104
- Ueda, Y., Akiyama, M., Ohta, K., & Miyaji, T. 2003, *ApJ*, **598**, 886
- Ueda, Y., Hiroi, K., Isobe, N., et al. 2011, *PASJ*, **63**, S937
- Uematsu, R., Ueda, Y., Tanimoto, A., et al. 2021, *ApJ*, **913**, 17
- Urry, C. M., & Padovani, P. 1995, *PASP*, **107**, 803
- Vander Meulen, B., Camps, P., Stalevski, M., & Baes, M. 2023, *A&A*, **674**, A123
- Vasudevan, R. V., & Fabian, A. C. 2007, *MNRAS*, **381**, 1235
- Venanzi, M., Hönig, S., & Williamson, D. 2020, *ApJ*, **900**, 174
- Wittkowski, M., Kervella, P., Arsenault, R., et al. 2004, *A&A*, **418**, L39
- Yamada, S., Ueda, Y., Herrera-Endoqui, M., et al. 2023, *ApJS*, **265**, 37
- Yamada, S., Ueda, Y., Tanimoto, A., et al. 2021, *ApJS*, **257**, 61
- Zhao, X., Marchesi, S., Ajello, M., Baloković, M., & Fischer, T. 2020, *ApJ*, **894**, 71
- Zhuang, M.-Y., Ho, L. C., & Shanguan, J. 2018, *ApJ*, **862**, 118